



**HAL**  
open science

## **Bismuth coated graphite felt modified by silver particles for selective electroreduction of CO<sub>2</sub> into formate in a flow cell**

Yaoyin Lou, Dong Fu, Bruno Fabre, Florence Fourcade, Abdeltif Amrane, Mathieu Pasturel, Riadh Bourzami, Odile Merdrignac-Conanec, Thierry Labasque, Florence Geneste

► **To cite this version:**

Yaoyin Lou, Dong Fu, Bruno Fabre, Florence Fourcade, Abdeltif Amrane, et al.. Bismuth coated graphite felt modified by silver particles for selective electroreduction of CO<sub>2</sub> into formate in a flow cell. *Electrochimica Acta*, 2021, 371, pp.137821. 10.1016/j.electacta.2021.137821 . insu-03116010

**HAL Id: insu-03116010**

**<https://insu.hal.science/insu-03116010>**

Submitted on 20 Jan 2021

**HAL** is a multi-disciplinary open access archive for the deposit and dissemination of scientific research documents, whether they are published or not. The documents may come from teaching and research institutions in France or abroad, or from public or private research centers.

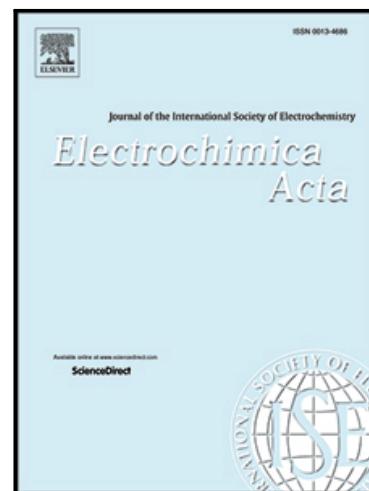
L'archive ouverte pluridisciplinaire **HAL**, est destinée au dépôt et à la diffusion de documents scientifiques de niveau recherche, publiés ou non, émanant des établissements d'enseignement et de recherche français ou étrangers, des laboratoires publics ou privés.

## Journal Pre-proof

Bismuth coated graphite felt modified by silver particles for selective electroreduction of CO<sub>2</sub> into formate in a flow cell

Yaoyin Lou , Dong Fu , Bruno Fabre , Florence Fourcade ,  
Abdeltif Amrane , Mathieu Pasturel , Riadh Bourzami ,  
Odile Merdrignac-Conanec , Thierry Labasque , Florence Geneste

PII: S0013-4686(21)00110-9  
DOI: <https://doi.org/10.1016/j.electacta.2021.137821>  
Reference: EA 137821



To appear in: *Electrochimica Acta*

Received date: 23 September 2020  
Revised date: 4 December 2020  
Accepted date: 13 January 2021

Please cite this article as: Yaoyin Lou , Dong Fu , Bruno Fabre , Florence Fourcade , Abdeltif Amrane , Mathieu Pasturel , Riadh Bourzami , Odile Merdrignac-Conanec , Thierry Labasque , Florence Geneste , Bismuth coated graphite felt modified by silver particles for selective electroreduction of CO<sub>2</sub> into formate in a flow cell, *Electrochimica Acta* (2021), doi: <https://doi.org/10.1016/j.electacta.2021.137821>

This is a PDF file of an article that has undergone enhancements after acceptance, such as the addition of a cover page and metadata, and formatting for readability, but it is not yet the definitive version of record. This version will undergo additional copyediting, typesetting and review before it is published in its final form, but we are providing this version to give early visibility of the article. Please note that, during the production process, errors may be discovered which could affect the content, and all legal disclaimers that apply to the journal pertain.

© 2021 Published by Elsevier Ltd.

## Highlights

- A new Bi-coated graphite felt decorated with silver particles was prepared.
- The parameters of the spontaneous deposition were optimized to achieve a homogenous material.
- The bimetallic electrode exhibited high selectivity of 88% for formate production.
- Ag and Bi played a complementary role instead to perform competitive reactions.
- The high performance of the electrode evidenced its potential for CO<sub>2</sub> reduction.

Journal Pre-proof

Bismuth coated graphite felt modified by silver particles for selective  
electroreduction of CO<sub>2</sub> into formate in a flow cell

Yaoyin Lou<sup>a,b</sup>, Dong Fu<sup>a</sup>, Bruno Fabre<sup>a</sup>, Florence Fourcade<sup>b</sup>, Abdeltif Amrane<sup>b</sup>, Mathieu Pasturel<sup>a</sup>, Riadh Bourzami<sup>d</sup>, Odile Merdrignac-Conanec<sup>a</sup>, Thierry Labasque<sup>c</sup>, Florence Geneste<sup>a,\*</sup>

<sup>a</sup> Univ Rennes, CNRS, ISCR-UMR 6226, F-35000 Rennes, France

<sup>b</sup> Univ Rennes, Ecole Nationale Supérieure de Chimie de Rennes, CNRS, ISCR-UMR 6226, F-35000 Rennes, France

<sup>c</sup> Géosciences Rennes-OSUR, UMR CNRS 6118, université de Rennes 1, France

<sup>d</sup> Research unit of emergent materials, Ferhat Abbas, Sétif-1 university, Sétif, Algeria

ABSTRACT

A 3D porous Ag-Bi electrode was developed to achieve the highly selective reduction of CO<sub>2</sub> into formate. Ag particles were deposited on Bi coated graphite felt by galvanic displacement reaction. The selectivity of the reduction was enhanced with the Ag-Bi electrode compared with Bi coated graphite felt. The bimetallic catalytic system converted CO<sub>2</sub> into formate with a high selectivity of 88% at -1.6 V<sub>SCE</sub>. The highly porous structure and large surface area of the electrode facilitated the mass transport, leading to a high surface current density of 76 mA cm<sup>-2</sup> and a production rate of 8.1 ± 0.4 mmol cm<sup>-3</sup> h<sup>-1</sup> (62 ± 3 mg cm<sup>-2</sup> h<sup>-1</sup>). These results are very promising in the context of the electrochemical conversion of CO<sub>2</sub>.

---

\* florence.geneste@univ-rennes1.fr

Keywords: CO<sub>2</sub> reduction, Ag-Bi electrode, galvanic displacement reaction, bimetallic catalyst, flow electrochemical cell

## 1. Introduction

The continuous increase of greenhouse gas CO<sub>2</sub> content in atmosphere has generated high interest into efficient methods allowing its conversion and valorization. Among them, electrochemistry is a highly interesting alternative since it can convert CO<sub>2</sub> into useful fuels and chemicals and can be directly integrated with renewable resources. The reduction of CO<sub>2</sub> into CO<sub>2</sub><sup>-</sup> occurs at a very negative potential (-1.9 V vs Standard Hydrogen Electrode SHE at pH 7 [1]) in aqueous medium and a catalyst is therefore necessary to decrease the overpotential. Many different metal electrodes have shown high catalytic ability to reduce CO<sub>2</sub> with however different selectivity [2, 3]. Thus, copper can reduce CO<sub>2</sub> into multicarbon products [4], whereas gold and silver usually yield carbon monoxide [5-9]. Bismuth (Bi) considered as a cost-effective and environmentally friendly electrode material is also a promising catalyst for CO<sub>2</sub> reduction, leading to CO or formate depending on the nature of the electrolytic medium [10-14]. A current density of 57 mA cm<sup>-2</sup> at -1.16 V vs Reversible Hydrogen Electrode (RHE) with a Faradaic efficiency (FE) for formate of 95% was achieved in CO<sub>2</sub>-saturated aqueous HCO<sub>3</sub><sup>-</sup> solution with a Bi electrode having short inter-layer Bi-Bi bonds [15].

Some bimetallic electrodes have also shown higher catalytic activities compared with their pure metal counterparts [16-18]. In that context, Ag has been associated to Cu in order to improve the catalytic performance for CO<sub>2</sub> reduction due to a tandem sequential catalysis and electronic effect [19, 20]. Bimetallic electrodes containing Bi have also been studied [21-25].

An increase in FE has been obtained with Cu-Bi electrodes, which was attributed to a change in the local environment of Bi modulated by Cu atoms [21]. A synergistic effect has also been observed between Bi and Mo for producing methanol [23]. S-O composite involving a bimetallic Ag-Bi system has also improved Faradaic efficiency for the selective CO<sub>2</sub> reduction into formate. The authors attributed the higher FE to the acceleration of H<sub>2</sub>O dissociation improved by the presence of Ag that increased the current density and local pH [25].

To approach the performance allowing the system to be used industrially (200 mA cm<sup>-2</sup> and FEs higher than 90%) [26] flow systems have also been considered as they improve both mass transport and current densities [15, 27]. Since the recycling of the solution through the electrode can be avoided, they also limit the variation of pH that occurs unavoidably during bulk electrolysis. It avoids a continuous formation of hydroxide ions if hydrogen evolution occurs and so their subsequent reaction on dissolved CO<sub>2</sub> to form carbonates [27, 28].

In the pursuit of our investigations on the modification of graphite felts and their use in depollution processes [29-31], Bi coated graphite felts with high surface area and good stability [32] were prepared and their high catalytic activity toward the reductive dechlorination of chloroacetamides was highlighted [33]. Herein, Bi modified graphite felts were used in a flow system for CO<sub>2</sub> reduction. The electrode was modified with silver particles by galvanic displacement reaction to give rise to a new bimetallic porous electrode material, advantageously prepared from low-cost and large-scale available graphite felt. Whereas CO<sub>2</sub> reduction on Ag is known to give CO as the main product, an improvement in the FE for formate has been obtained with the bimetallic system, although the electrode did not contain sulfur modifiers as reported before [25]. This porous Ag-Bi electrode of high specific surface area, which is easy and cost-effective to produce, is highly suitable for flow systems and allowed the achievement of high current densities and high production rate.

## 2. Materials and methods

### 2.1. Chemicals and materials

Bismuth(III) oxide ( $\text{Bi}_2\text{O}_3$ ) was purchased from Acros Organics. Nitric acid ( $\text{HNO}_3$ ), anhydrous sodium sulfate ( $\text{Na}_2\text{SO}_4$ , 99%), silver nitrate ( $\text{AgNO}_3$ ) and 2,2-bis(hydroxymethyl)-2,2',2'-nitrilotriethanol ( $(\text{HOCH}_2)_3\text{CN}(\text{CH}_2\text{CH}_2\text{OH})_2$ , TEA), 98+%, were purchased from Alfa Aesar®. Graphite felt (GF, Recycled vein graphite RVG 4000) was supplied by Mersen (France). PVP (polyvinylpyrrolidone, molecular weight 25,000) was provided by E. Merck (Germany). Sodium hydroxide ( $\text{NaOH}$ ) was purchased from AnalaR NORMAPUR®.

### 2.2. Preparation of Bi coated graphite felts and further modified with Ag particles (Ag-Bi@GF)

Ag-Bi@GF was prepared by electroless deposition of silver particles on Bi coated graphite felt (Bi@GF).

Bi@GF was prepared as previously reported (Bi graphite felt cuboid : 11 cm × 6 cm, 3 mm thickness) [32]. The deposition of Ag particles onto Bi@GF was carried on a sample (1 cm diameter, 1.5 mm thickness) taken from the Bi graphite felt cuboid, by galvanic displacement reaction (equation 1) according to a previous study [34] and modified as follows: first, Bi@GF was etched under sonication in 0.1 mol L<sup>-1</sup>  $\text{HNO}_3$  for 5 minutes, and then rinsed with water three times for 5 min. Then, the electrode (diameter: 1 cm; thickness: 1.7 mm) was cycled (6 scans) by cyclic voltammetry from -0.6 to -1 V vs MSE in 0.1 mol L<sup>-1</sup>  $\text{HNO}_3$ . The electrode was then dipped for 20-45 min in 25 mL of a solution at 0.5-2.0 mmol L<sup>-1</sup>  $\text{AgNO}_3$  and 0-1.3 mmol L<sup>-1</sup> (0-0.4 g, 25000 g mol<sup>-1</sup>) PVP previously degassed for 1h prior to Ag deposition, kept under argon at  $25 \pm 0.1^\circ\text{C}$  and stirred at 250 rpm with a magnetic stirrer.



### 2.3. Flow electroreduction of CO<sub>2</sub>

CO<sub>2</sub> electroreduction was performed in a home-made flow cell (Fig. S1) [35]. To ensure a good homogeneity of the potential distribution in the three dimensional working electrode Bi@GF and Ag-Bi@GF working electrodes (diameter: 1 cm; thickness: 1.5 mm) were positioned between two interconnected DSA (dimensionally stable anodes) counter-electrodes (AC-2004, supplied by ECS International Electro Chemical Services, France). The compartments were separated by cationic exchange membranes (Nafion™ 417 membrane, France). The reference electrode (mercury/mercurous sulfate – abbreviated as MSE) was positioned in the middle of the working electrode to limit the ohmic drop and the cathodic potential was applied using a VersaSTAT 3 potentiostat from Ametek/Princeton Applied (Elancourt, France). The electrodes were pre-treated in the flow cell by electroreduction at -1.1 V<sub>SCE</sub> until the current was constant (for 1-2h) in 0.1 mol L<sup>-1</sup> Na<sub>2</sub>SO<sub>4</sub> and then washed with ultrapure water. This pre-treatment was necessary to eliminate oxides formed at the surface of Bi electrode [33]. The 0.5 mol L<sup>-1</sup> KHCO<sub>3</sub> solution was saturated with CO<sub>2</sub> for 30 min before to be pumped through the electrochemical cell. The Faradaic efficiency FE was calculated as follows:

$$\text{Faradaic efficiency} = NF \frac{n}{Q} \times 100 \quad (2)$$

where  $N$  is the number of moles of consumed electrons ( $N(\text{H}_2) = 2$ ,  $N(\text{HCOO}^-) = 2$ ,  $N(\text{CO}) = 2$ ),  $F$  is the Faraday constant (96 500 C mol<sup>-1</sup>),  $n$  is the amount of generated HCOO<sup>-</sup>, H<sub>2</sub> or CO (mol), and  $Q$  is the consumed electrical charge (C).

The volume current density  $J$  was calculated according to the following equation:

$$J = I/V \quad (3)$$

Where  $I$  is the current (A) and  $V$  the volume of the 3D porous electrode (0.13 cm<sup>3</sup>).

To compare to 2D electrodes, the surface current density was also given considering the geometrical surface area of the electrode ( $0.78 \text{ cm}^2$ ).

#### 2.4. Additional instrumentation

For X-ray measurements, the samples were placed on Poly(methyl methacrylate) (PMMA) sample holders and fastened without strong compression below a Mylar foil. The powder diffraction patterns were measured using a Bruker D8 Advance diffractometer working with monochromatized  $\text{CuK}\alpha 1$  radiation ( $\lambda=1.5406 \text{ \AA}$ ) and equipped with a LynxEye fast detector. The diffraction patterns were measured from  $20^\circ$  to  $120^\circ$  with  $2\theta$  steps of  $0.02^\circ$  and integrated counting time of 250 s/step. The patterns were refined by the Rietveld method using the Fullprof software. For bismuth, the trigonal R-3m space group (no. 166) was considered with a single  $6c$  (0 0 z) Wyckoff position occupied by Bi-atoms while a cubic unit cell (Fm-3m space group, no. 225) with a single  $4a$  (0 0 0) Wyckoff position was used for silver.

Using a Thompson-Cox-Hastings peak profile function and taking into account the instrumental contribution of the apparatus measured on a corundum standard sample, the average crystallite size was extracted from the refinements.

Nitrogen adsorption isotherms were recorded at liquid nitrogen temperature (77K) using a Micromeritics Gemini VII Surface Area and Porosity Analyzer. Prior to adsorption, the electrode material was outgassed overnight under vacuum at room temperature to remove all physisorbed material. Specific surface areas (SSA) were calculated by Brunauer–Emmett–Teller (BET) method from  $\text{N}_2$  adsorption data in the relative pressure range 0.05–0.25.

The surface morphology of electrode materials was analyzed by JSM-7100F Field Emission Scanning Electron microscopy equipped by EDS (Energy Dispersive X-Ray Spectroscopy) Detector SDD type (Silicon Drift Detector) X-Max 80 mm<sup>2</sup> Oxford Instruments AZtecEnergy. Accelerating voltage was 10 kV with a beam current of 1 nA and a spectra collection time of 100 s.

Gas chromatography (GC) measurements for the detection and quantification of the gas produced from electrolysis (e.g. CO and H<sub>2</sub>) were performed with a PerkinElmer® Clarus® 580 gas chromatograph equipped with two detectors: a Thermal Conductivity Detector (TCD) and a Flame Ionization Detector (FID), and two columns: a Restek® Haysep Q (1 mm × 2 m) micropacked column and a Restek® ShinCarbon ST (1 mm × 2 m) micropacked column. The detection of gaseous products was carried out at a TCD temperature of 50°C and a FID temperature of 380°C. A calibration plot was first performed with a calibrated mixture of gases containing H<sub>2</sub> (10 %, v/v), CO (10 %, v/v), CH<sub>4</sub> (5 %, v/v), CO<sub>2</sub> (20 %, v/v), and He (55 %, v/v) (from Air Products). To assure a constant pressure in the receiving flask, a water displacement system was implemented. The gas was collected at the end of the electrolysis with a gas-tight syringe from the gas phase of the receiving flask and immediately injected in the gas chromatograph.

The concentration of formate was determined using DIONEX DX120 ion chromatography equipped with a conductivity detector and a DIONEX AS19 (4 × 250 mm) ion-exclusion column. The sample was eluted with potassium hydroxide at a flow rate of 1 mL min<sup>-1</sup>. The detection was carried out by conductivity with a Self-Regenerating Suppressor (SRS).

Linear voltammetry analyses were performed with a VersaSTAT3 AMETEK Model (Princeton Applied Research) potentiostat/galvanostat. A standard three-electrode glass electrochemical cell was used in which were inserted GF (4 mm diameter, 1.7 mm thickness), Bi@GF (2.5 mm diameter, 1.7 mm thickness) or Ag-Bi@GF (2.5 mm diameter, 1.7 mm thickness) as the working electrode, a platinum plate as the auxiliary electrode, and a KCl-saturated calomel electrode (SCE) as the reference electrode. The electrolytic solution was 0.5 mol L<sup>-1</sup> KHCO<sub>3</sub> (pH 7.2) under CO<sub>2</sub> or Ar saturation.

### 3. Results and discussion

#### 3.1. Preparation of Ag-Bi@GF

##### 3.1.1. Preliminary cyclic voltammetry analysis

The Ag deposition onto the Bi surface was performed by galvanic displacement reaction according to equation 1, whose reaction rate is highly dependent on the difference between the reduction potential of  $\text{Ag}^+$  and the oxidation potential of Bi in the studied medium. The partial reactions of the Ag/Bi galvanic exchange, including Bi electrodisolution and Ag deposition, were studied by linear voltammetry (Fig. 1). The potential overlap for which both Ag deposition and Bi dissolution could occur simultaneously was 230 mV, and decreased to 122 mV in the presence of PVP (Fig. 1). Indeed, the redissolution of bismuth occurred at a less negative potential when PVP was added to the solution, probably due to the adsorption of the polymer onto the Bi surface.

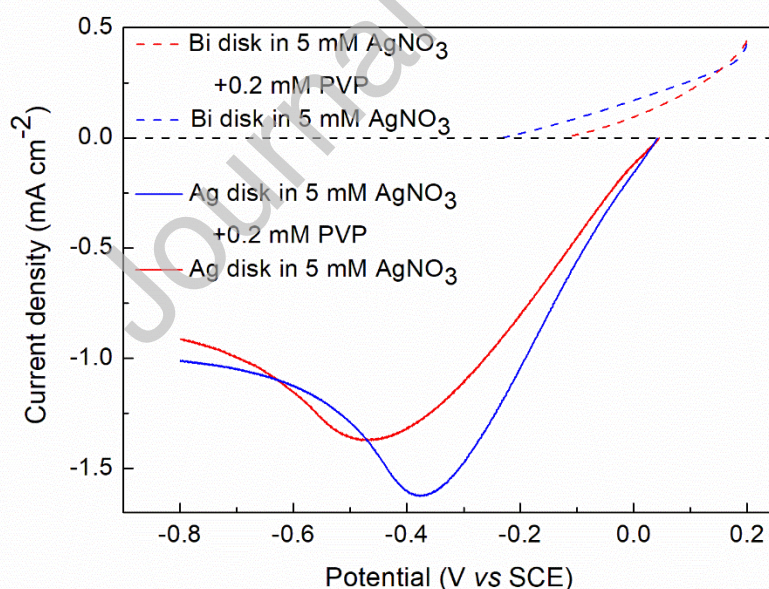


**Fig. 1.** Linear sweep voltammograms of the Bi electrodisolution and the Ag deposition in 5 mmol L<sup>-1</sup> AgNO<sub>3</sub>. The detailed composition of the solutions is reported on the figure. Anodic

and cathodic curves were recorded with Bi and Ag disk electrodes, respectively. Scan rate: 0.1 V s<sup>-1</sup>.

This medium was used for the Ag deposition and the concentrations of PVP and Ag<sup>+</sup> ions were optimized to obtain a high density of nanoparticles homogeneously distributed inside the three dimensional electrode. Main experimental results are summarized in Table S1.

### *3.1.2. Pretreatment of Bi@GF*

Before deposition, Bi@GF was sonicated in nitric acid and underwent an electrochemical treatment to smooth the surface and eliminate oxides (Fig. 2a, b). This pretreatment had a significant impact on the subsequent Ag deposition since a lower density of silver was found on the untreated Bi@GF (Fig. 2 c, d). Indeed, some black areas identified as silver particles by EDS (Fig. S2) were present on the untreated material (Fig. 2c), whereas the treated material showed a high density of Ag plates (Fig. 2d). This pretreatment was therefore used in the following experiments.

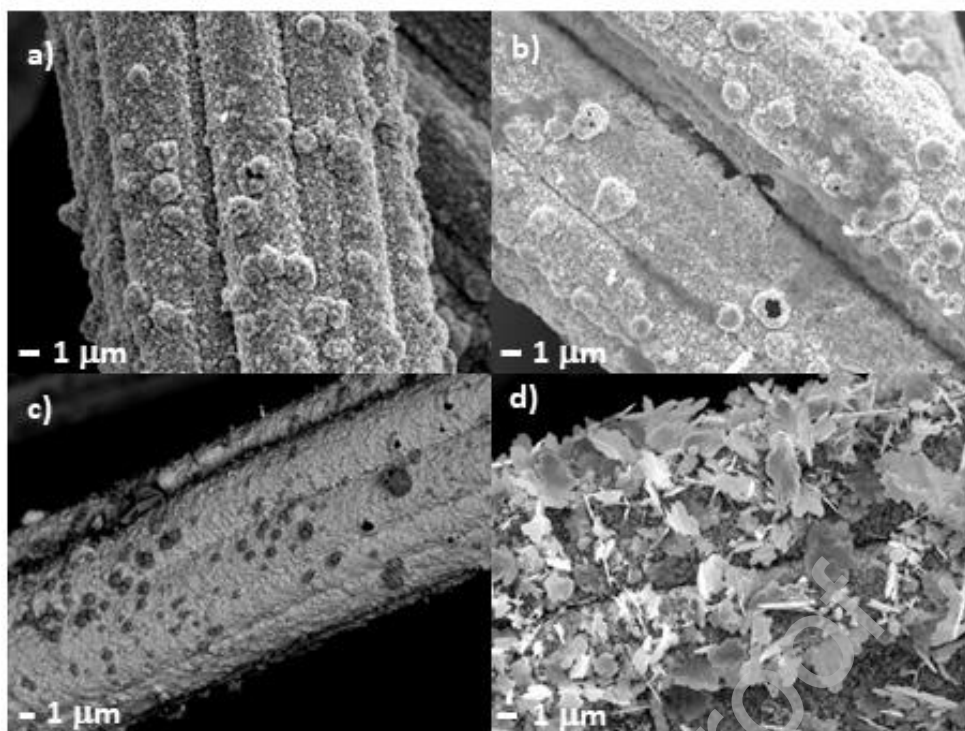


**Fig. 2.** SEM images of Bi@GF (a,b) and Ag-Bi@GF (c,d) with (b,d) and without (a,c) acid washing and electrochemical pretreatment of Bi@GF. Ag deposition was performed in  $2 \text{ mmol L}^{-1} [\text{AgNO}_3]$ , for 45 min.

### 3.1.3. Effect of PVP on the Ag deposition

PVP polymer has demonstrated its ability as stabilizing agent to promote the formation of well-defined Ag nanostructures in electroless processes [36] and electrodeposition [37]. It has been also reported that PVP favours the nucleation of Ag clusters on the surface [38]. The addition of PVP during the modification step of the Bi@GF significantly reduced the size of the Ag plates formed on the surface (Fig. 3 a, b), which were around  $1\text{-}2 \mu\text{m}$  against  $4\text{-}5 \mu\text{m}$  without PVP (Fig. 2d). However, when the concentration of PVP was increased to  $1.3 \text{ mmol L}^{-1}$ , the Ag plates grew again (Fig. 3c). Therefore, a concentration of  $0.3 \text{ mmol L}^{-1}$  of PVP was used in the following experiments to preclude the formation of fragile larger Ag plates.

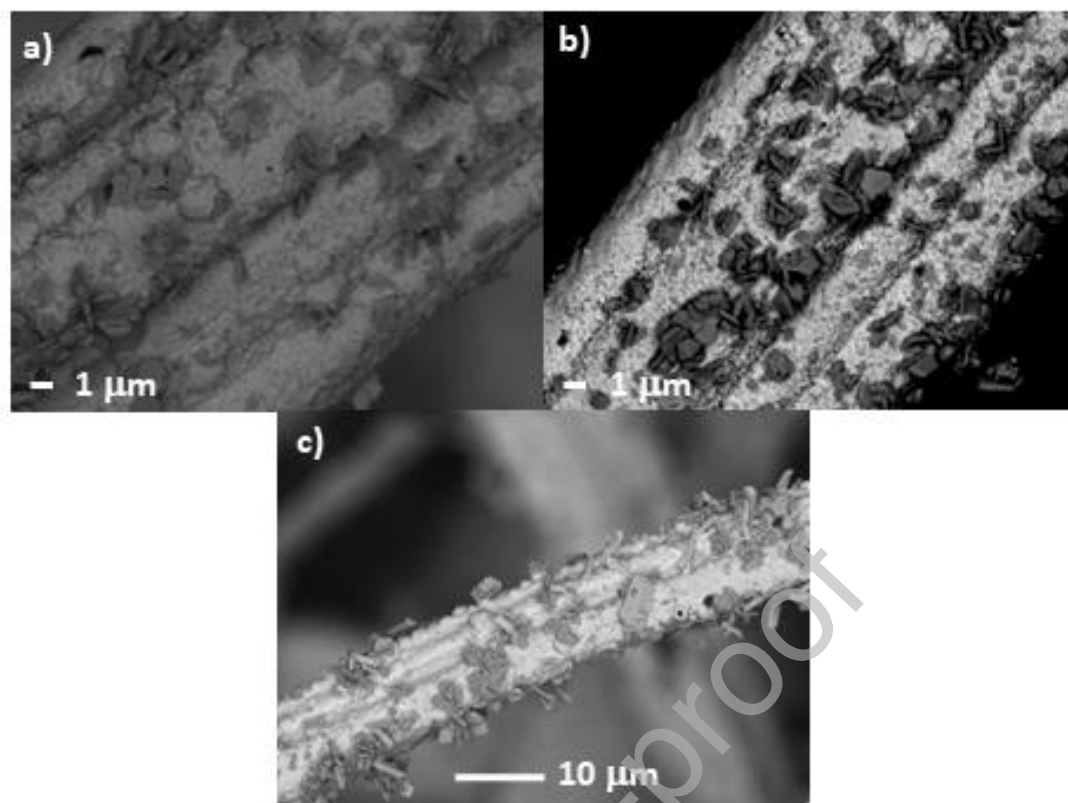


**Fig. 3.** SEM images of Ag-Bi@GF prepared from a solution containing  $2 \text{ mmol L}^{-1} \text{ AgNO}_3$  and  $0.32$  (a);  $0.64$  (b) or  $1.25 \text{ mmol L}^{-1} \text{ PVP}$  (c). Deposition time: 45 min.

#### 3.1.4. Effect of $\text{Ag}^+$ concentration and deposition time

To decrease the size of the deposited Ag plates, the concentration of the silver salt was decreased to  $1 \text{ mmol L}^{-1}$  and different deposition times were tested from 20 to 45 min (Fig. 4). SEM images showed that the effect of the decreasing silver concentration was not obvious, whereas the deposition time had a great influence on the size of the Ag particles. Indeed, 45 min led to ca.  $1 \mu\text{m}$  long Ag plates (Fig. 4 a,b), whereas 30 and 20 min times led to Ag particles ranging approximately from 200 to 400 nm size (Fig. 4 c to e). Twenty min was thus selected to deposit silver on Bi@GF since the density of Ag particles was lower in that

case, yielding a more homogenous material with less aggregation of silver particles. It is worth noting that an increase of the silver concentration to  $2 \text{ mmol L}^{-1}$  led to the formation of Ag plates even when 20 min deposition time was used (Fig. S3).

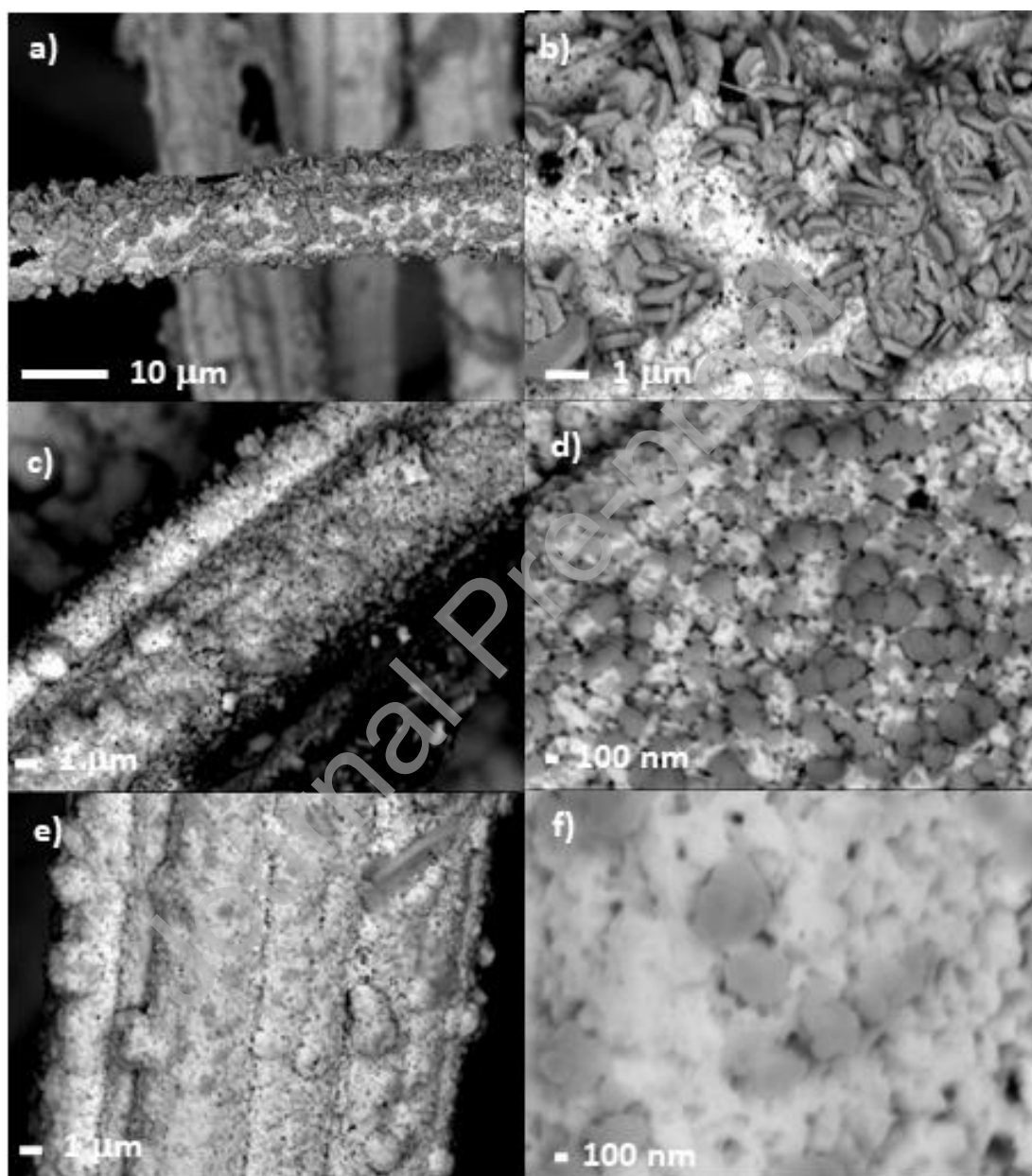


**Fig. 4.** SEM images of Ag-Bi@GF prepared from a solution containing  $1 \text{ mmol L}^{-1} \text{ AgNO}_3$  and  $0.32 \text{ mmol L}^{-1} \text{ PVP}$ . Deposition time: 45 (a, b), 30 (c, d) and 20 min (e, f).

### 3.1.5. Characterization of Ag-Bi@GF

The X-ray diffraction (XRD) patterns of Bi@GF and Ag-Bi@GF (prepared from a solution containing 1 mmol L<sup>-1</sup> AgNO<sub>3</sub>, 0.32 mmol L<sup>-1</sup> PVP and a 20 min deposition time) are shown in Fig. 5 and a summary of crystallographic data is given in Table 1.

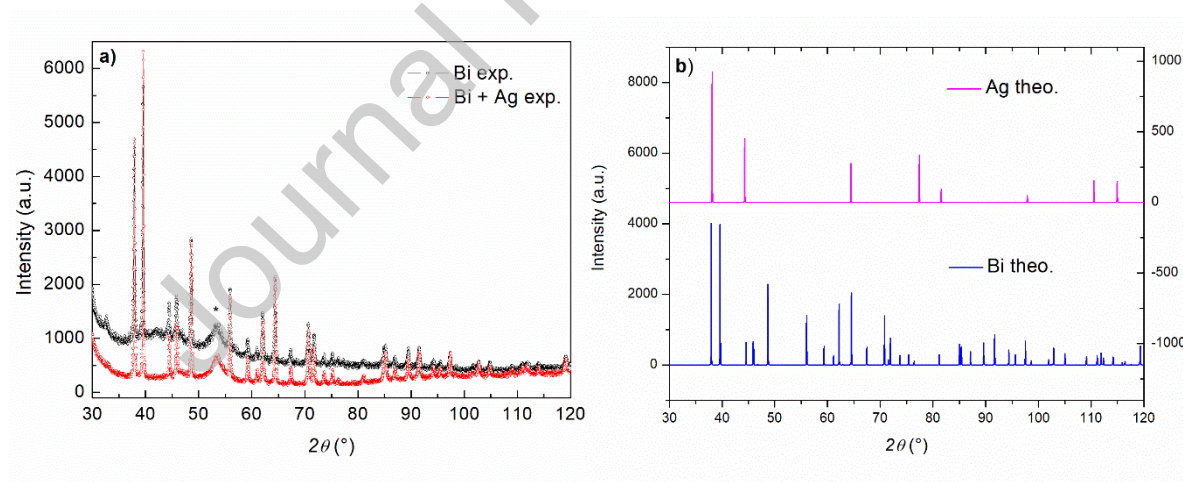
**Table 1**

Results of Rietveld refinements for Bi@GF and Ag-Bi@GF electrodes

Sample	Bi@GF	Ag-Bi@GF
Bi cell parameters (Å)	a = 4.5481(1) c = 11.8613(3) (hexagonal settings)	a = 4.5469(2) c = 11.8574(4)
Bi Wyckoff position	0 0 0.2341(1)	0 0 0.2338(1)
Ag cell parameter (Å)	-	a = 4.0881(4)
Average	345(10)	322(10)
Bi crystallite diameter (Å)		
2θ range (°)	30-120	30-120
Reflections/parameters	59 / 10	59 + 8 / 13
Reliability factors	χ <sup>2</sup>	1.49
	Rp	20.5
	Rwp	17.5
	Rexp	12.4

Bi@GF was composed of pure metallic rhombohedral Bi with lattice parameters agreeing with literature data [39]. No significant change of the cell parameters was observed after Ag-deposition. The diffraction peaks characteristic from Ag, which are expected at 2θ = 38.0°, 44.2° and 64.5° (corresponding to the (111), (220) and (200) planes, respectively) were not clearly observed due to the presence of superimposed Bi peaks (Fig. 5b). However, the peaks at 77.4° and 81.5° corresponding to the (311) and (222) planes respectively were detected

(Fig. 5c), which confirmed the presence of silver on the electrode. No significant preferential orientation, neither for Bi nor for Ag, was detected by the XRD patterns refinement, in agreement with the rather isotropic shape of the metal particles observed on SEM images (Fig. 4). Investigation of the Bragg peak broadening lead to an average crystallite size for Bi of 345(10) Å and 322(10) Å before and after Ag-deposition, respectively. For Ag, the number of independent reflections was not sufficient to perform any precise analysis, but the broadening was constrained to that of Bi, leading to a rather satisfying description of the peak profile. From these sizes, one can conclude that most of bismuth visible on Fig. 4c are single crystallite or composed of 2-3 grains at maximum. Although Ag was detected by X-ray diffraction, the very small size of the peaks was not in accordance with the high amount of silver observed in SEM images (Fig. 4e). It indicated that Ag does not form a continuous layer on Bi surface but forms particles having mainly an amorphous character.



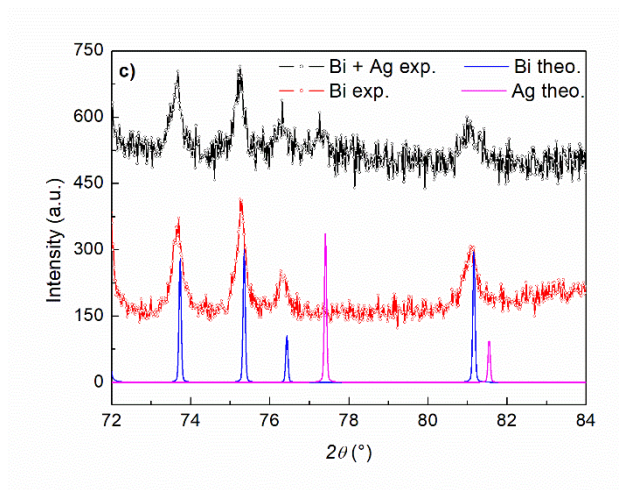


**Fig. 5.** Rietveld refined XRD patterns of Bi@GF and Ag-Bi@GF. The experimental data (a) are represented by red or black symbols and the calculated pattern (b) by blue and pink lines. The broad bump centered at  $53.5^\circ$ , marked by an asterisk, originates from the Mylar foil and was included into the background signal. (c) Comparison of both patterns in a selected  $2\theta$  range showing the presence of Ag Bragg peaks aside Bi ones.

The specific surface area ( $S_{\text{BET}}$ ) of Ag-Bi@GF was estimated to be  $4.5 \pm 0.2 \text{ m}^2 \text{ g}^{-1}$  by BET measurements and the average diameter of pores, supposedly of cylindrical shape, was  $87 \pm 3 \text{ \AA}$ . The  $S_{\text{BET}}$  value of Ag-Bi@GF was 10 times higher than that of Bi@GF, probably due to the increased roughness and porosity of the surface induced by the dissolution of bismuth during the modification of Bi@GF.

### 3.2. $\text{CO}_2$ electroreduction

#### 3.2.1. Linear voltammetry analysis

The catalytic activity of Bi@GF and Ag-Bi@GF electrodes towards the reduction of  $\text{CO}_2$  was investigated by linear voltammetry in  $\text{KHCO}_3$ -containing aqueous solution (pH 7.2) (Fig. 6).

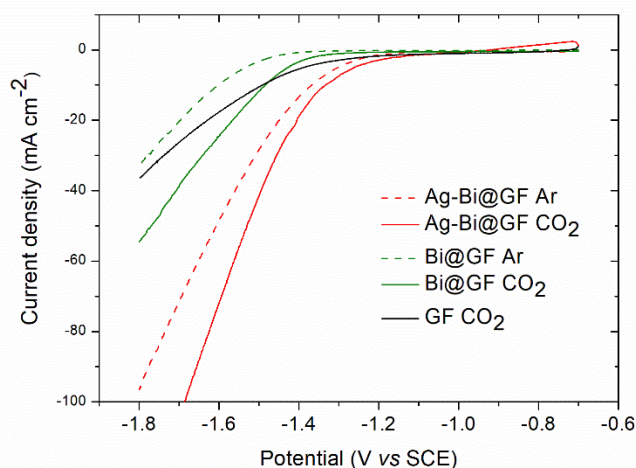


**Fig. 6.** Linear sweep voltammograms at  $100 \text{ mV s}^{-1}$  for GF (4 mm diameter, 1.7 mm thickness), Bi@GF (2.5 mm diameter, 1.7 mm thickness) and Ag-Bi@GF (2.5 mm diameter, 1.7 mm thickness) in  $0.5 \text{ mol L}^{-1} \text{ KHCO}_3$  (pH 7.2) under  $\text{CO}_2$  or Ar saturation.

The electrolytic medium has been chosen as pH buffer since  $\text{HCO}_3^-$  is known to increase the effective concentration of dissolved  $\text{CO}_2$  near the electrode surface through rapid equilibrium between bicarbonate and dissolved  $\text{CO}_2$  [40]. Since the repartition of the potential in a three-dimensional electrode is not homogeneous, it is difficult to estimate the exact value of the onset potential corresponding to the reduction of  $\text{CO}_2$ . Nonetheless, a value close to  $-1.3 \text{ V}_{\text{SCE}}$  ( $-1.05 \text{ V}_{\text{SHE}}$  at pH 7) can be deduced for Bi@GF from Fig. 6, which corresponds to a small overpotential around 0.4 V considering the standard potential of the  $\text{CO}_2/\text{HCOO}^-$  system ( $E^\circ(\text{CO}_2/\text{HCOO}^-) = -0.61 \text{ V}_{\text{SHE}}$  at pH 7 [41]). This value is consistent with those previously reported for other types of Bi electrodes [39, 42]. For Ag-Bi@GF the overpotential is even smaller with a 100 mV less negative onset potential. However, the competitive hydrogen evolution reaction occurred at less cathodic potential owing to the presence of silver. The catalytic activity of Bi@GF and Ag-Bi@GF towards  $\text{CO}_2$  reduction is clear if one compares

the linear voltammograms performed under argon. Moreover, the current densities were also more intense than those measured at the bare graphite felt for potentials lower than  $-1.5 \text{ V}_{\text{SCE}}$ .

### 3.2.2. *Effect of the applied potential*

The catalytic activity of Bi@GF and Ag-Bi@GF was then investigated by electrolysis tests in  $0.5 \text{ mol L}^{-1} \text{ KHCO}_3$  (pH 7.2) under  $\text{CO}_2$  saturation in a flow electrochemical cell (Fig. S1). For these first experiments, this home-made cell was used instead of the classical flow cell with gas-diffusion electrodes [43] since it has previously shown good performances for pollution treatment and it is well-adapted to three-dimensional porous electrode materials [29, 31, 33]. Since the reduction of  $\text{CO}_2$  on bismuth in aqueous medium is known to produce formate [13], the liquid phase was analyzed by ion chromatography (Fig. S4) and the potential-dependent Faradaic efficiency for formate is given in Fig. 7. The analysis of the gaseous phase by GC has also been carried out in order to detect the possible formation of CO and  $\text{H}_2$ .

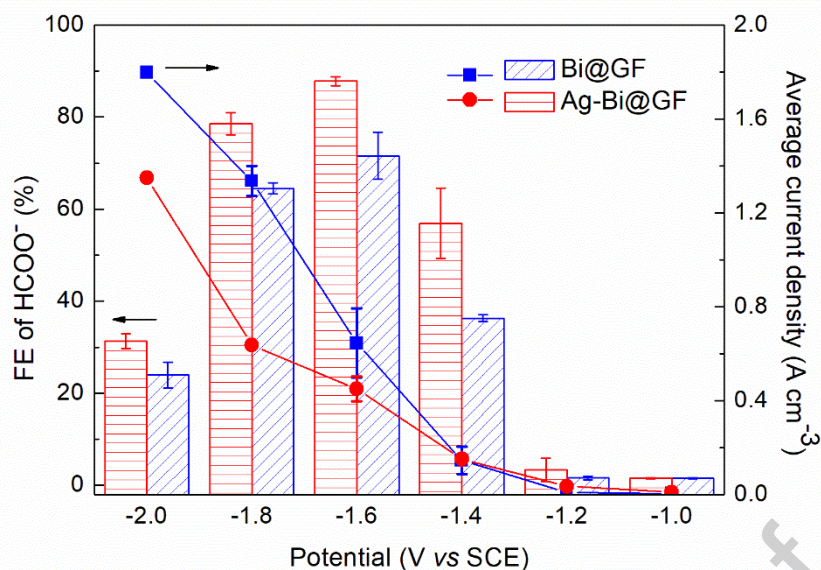


**Fig. 7.** Faradaic efficiency for  $\text{HCOO}^-$  production at Bi@GF (10 mm diameter, 1.7 mm thickness) and Ag-Bi@GF (10 mm diameter, 1.7 mm thickness) after 30 min electrolysis at different potentials in  $0.5 \text{ mol L}^{-1} \text{ KHCO}_3$  (pH 7.2) under  $\text{CO}_2$  saturation. Flow rate:  $2.5 \text{ mL min}^{-1}$ . Error bars are based on two experiments.

For Bi@GF, the highest FE for formate ( $72 \pm 5\%$ ) was obtained at a potential of  $-1.6 \text{ V}_{\text{SCE}}$ , which indicates that the reduction of  $\text{CO}_2$  predominates over hydrogen evolution at this potential. FE was lower than those previously reported with other Bi electrodes ( $> 90\%$ ) [15, 42], whereas the onset potential measured by cyclic voltammetry was quite similar. Since the Bi samples used to deposit silver particles were cut from a Bi graphite felt cuboid, it is likely that some carbon parts contained in such samples are not covered by bismuth. As a result, the presence of this carbonaceous material is probably responsible for the lower selectivity because it is well-known that the reduction of  $\text{CO}_2$  at carbon electrodes yields different by-products [44]. The average current densities were  $1.33 \pm 0.06 \text{ A cm}^{-3}$  ( $227 \pm 11 \text{ mA cm}^{-2}$ ) and  $0.6 \pm 0.1 \text{ A cm}^{-3}$  ( $110 \pm 25 \text{ mA cm}^{-2}$ ) at  $-1.8$  and  $-1.6 \text{ V}_{\text{SCE}}$ , respectively, which are among the

highest reported values for a bismuth electrode using CO<sub>2</sub>-saturated solutions [13, 15]. These results underline the benefit of using a porous electrode with a high surface area for electrocatalytic purposes.

Interestingly, the addition of Ag particles led to higher FE for formate (up to  $88 \pm 1\%$ ) compared with Bi alone for all applied potentials (Fig. 7), although the reduction of CO<sub>2</sub> at Ag is known to give usually CO [8]. Such a behaviour has been previously observed for CO<sub>2</sub> reduction at Ag-Bi-S-O composite electrode and attributed to a stronger absorption of reduced CO<sub>2</sub> intermediates on Bi than on Ag [25]. Indeed, the high affinity of Bi for the oxygen atom favours the formation of formate against CO [45]. This increase in selectivity corresponds to an increase in the amount of formed HCOO<sup>-</sup> for potentials of -1.2 and -1.4 V<sub>SCE</sub> (Table 2). The role of Ag particles would be to improve the charge-transfer process from electrode to the adsorbed CO<sub>2</sub> due to its high electrical conductivity (Fig. 8) [25]. However, for potentials more negative than -1.6 V<sub>SCE</sub>, the increase of FE is due to a lower volume current density obtained with Ag-Bi@GF compared with Bi@GF since less amount of formate was formed on Ag-Bi@GF. Such a result is however surprising since a higher current would be expected for the Ag-Bi@GF electrode owing to its higher specific surface area (its S<sub>BET</sub> value was 10 times higher compared with Bi@GF). The passivation of the Ag-Bi@GF electrode by the presence of oxides on its surface was also excluded since Ag-Bi@GF and Bi@GF electrodes were pre-treated before use by a reduction performed at a more cathodic potential (-1.1 V<sub>SCE</sub>) than the reduction potential of oxides on Bi [33] and Ag. A synergistic effect due to electronic interactions between Bi and Ag is unlikely owing to the absence of a crystal growth of Ag on Bi and to the amorphous character of deposited Ag particles, although *in situ* investigations would be necessary to confirm it. A possible explanation is the increase of local pH due to Ag particles, preventing H<sub>2</sub> from being released efficiently on Bi [25] and/or the formation of bubbles on the fibers surface, decreasing the active surface area of the electrode.

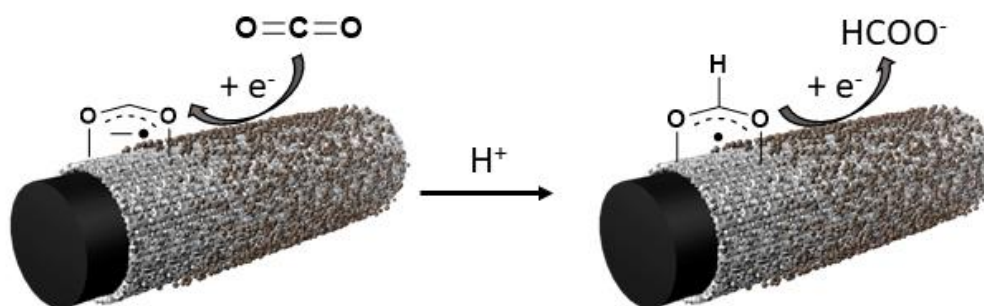


**Fig. 8.** Proposed mechanism for the selective reduction of  $\text{CO}_2$  at the bimetallic electrode

**Table 2**

Production yield for  $\text{HCOO}^-$  vs applied potential during 30 min electrolysis in  $0.5 \text{ mol L}^{-1}$   $\text{KHCO}_3$  (pH 7.2) under  $\text{CO}_2$  saturation. Error bars are based on two experiments.

Potential ( $V_{\text{SCE}}$ )	Bi@GF		Ag-Bi@GF	
	Faradaic efficiency (%)	$\text{HCOO}^-$ ( $\mu\text{mol}$ )	Faradaic efficiency (%)	$\text{HCOO}^-$ ( $\mu\text{mol}$ )
-1.0	$1.5 \pm 0.1$	$0.085 \pm 0.006$	$1.5 \pm 0.1$	$0.2 \pm 0.02$
-1.2	$1.6 \pm 0.4$	$0.17 \pm 0.05$	$3 \pm 3$	$2 \pm 1$
-1.4	$36.3 \pm 0.7$	$65 \pm 25$	$57 \pm 8$	$107 \pm 13$
-1.6	$70 \pm 6$	$555 \pm 77$	$88 \pm 1$	$491 \pm 53$
-1.8	$64 \pm 1$	$1056 \pm 19$	$79 \pm 2$	$623 \pm 19$

The average total surface current density measured for Ag-Bi@GF reached 76 and 107  $\text{mA cm}^{-2}$  at -1.6 and -1.8  $V_{\text{SCE}}$ , respectively (Fig. 9), which is very promising for a  $\text{CO}_2$ -saturated solution at atmospheric pressure [21-23] although the value is lower than the critical one usually admitted for practical applications [26].

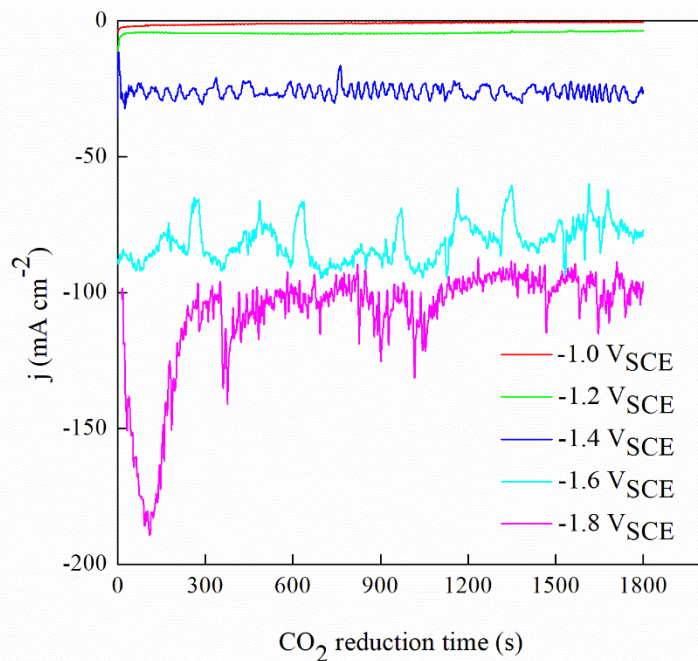


**Fig. 9.** Total surface current density measured for Ag-Bi@GF ( $\varnothing$  10 mm  $\times$  1.7 mm) vs electrolysis time at different applied potentials in 0.5 mol L<sup>-1</sup> KHCO<sub>3</sub> (pH 7.2) under CO<sub>2</sub> saturation.  $j$  was calculated from the geometrical disk surface area.

The influence of the flow rate on the FE for formate was examined for the Ag-Bi@GF electrode (Fig. 10). FE for formate was similar considering the standard deviation of FE for the studied range of flow rates.

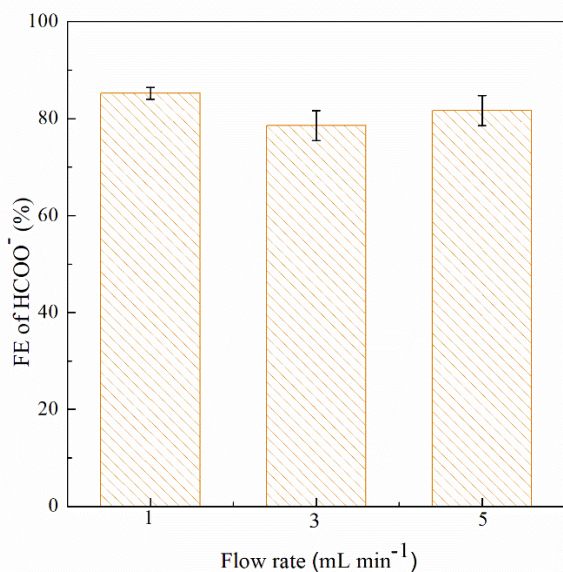


**Fig. 10.** Histograms of Faradaic efficiencies vs flow rate for the electrochemical reduction of CO<sub>2</sub> to HCOO<sup>-</sup> at  $-1.6 V_{SCE}$  at the Ag-Bi@GF electrode in  $0.5 \text{ mol L}^{-1} \text{ KHCO}_3$  (pH 7.2) under CO<sub>2</sub> saturation with one pass through the electrode. Error bars are based on two experiments.

A comparison of the catalytic activities of Bi@GF and Ag-Bi@GF towards CO<sub>2</sub> reduction was performed in the optimized conditions (i.e.,  $-1.6 V_{SCE}$  and  $1 \text{ mL min}^{-1}$ ).

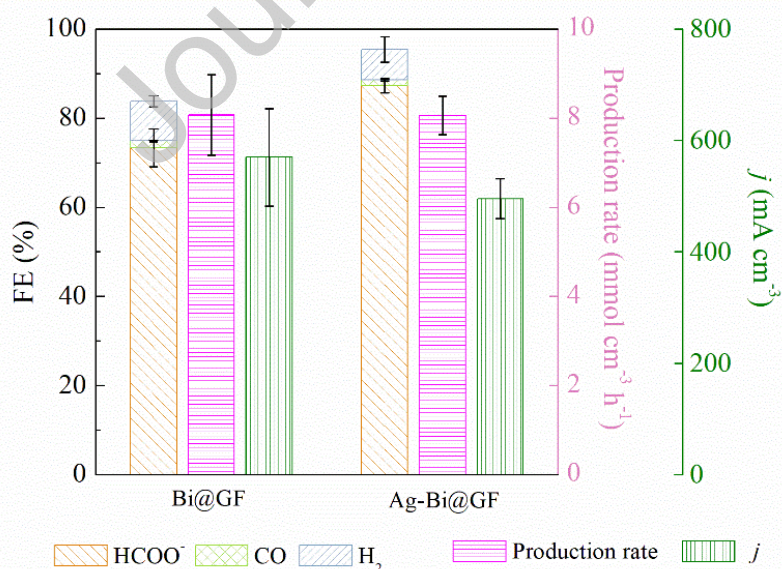


**Fig. 11.** Faradaic efficiencies, production rates and average current densities for electrochemical reduction of CO<sub>2</sub> at -1.6 V<sub>SCE</sub> on Bi@GF and Ag-Bi@GF electrodes in 0.5 mol L<sup>-1</sup> KHCO<sub>3</sub> (pH 7.2) under CO<sub>2</sub> saturation. Flow rate: 1 mL min<sup>-1</sup>. Error bars are based on two measurements.

As observed in Fig. 11, FE for formate was significantly higher with Ag-Bi@GF than with Bi@GF as previously observed with a flow rate of 2.5 mL min<sup>-1</sup> (Fig. 7). The amounts of CO and H<sub>2</sub> produced during the reduction of CO<sub>2</sub> at Ag-Bi@GF and Bi@GF were measured by GC (Fig. S5). The amount of formed CO was very low with a FE of 1-2% for both Bi@GF and Ag-Bi@GF electrodes, confirming that the presence of Ag did not yield a higher amount of CO. Even if hydrogen evolution occurred earlier on Ag, the FE for H<sub>2</sub> was only slightly higher on Bi@GF with 9 ± 1%, against 7 ± 3% for Ag-Bi@GF. Thus, the presence of Ag on the Bi coated GF significantly improved the FE for formate instead of increasing CO and H<sub>2</sub> production.

Under our electrocatalytic conditions (-1.6 V<sub>SCE</sub>), the lower current densities measured for Ag-Bi@GF compared with Bi@GF together with almost identical production rate of formate for both electrodes (namely, 8.1 ± 0.9 mmol cm<sup>-3</sup> h<sup>-1</sup>) led to a higher FE for formate of the Ag-Bi@GF electrode (Fig. 11). These results confirm that for electrolyses performed at -1.6 V<sub>SCE</sub>, the presence of Ag on the electrode did not lead to an increased amount of formed CO but to a higher FE for formate due to a lower volume current density.

### 3.2.3. Stability of Ag-Bi@GF in operation

The stability of Ag-Bi@GF was examined by performing seven successive cathodic electrolyses at -1.6 V<sub>SCE</sub> with the same electrode material and replacing the electrolytic

solution after each electrolysis. After seven electrolyses,  $44 \text{ mmol cm}^{-3}$  of  $\text{HCOO}^-$  were accumulated (Fig. 12). However, the FE for formate decreased significantly from 85% to 78% after the second electrolysis, and then decreased more slightly until reaching 70% after the last electrolysis. The FE for  $\text{H}_2$  slightly increased after each electrolysis.

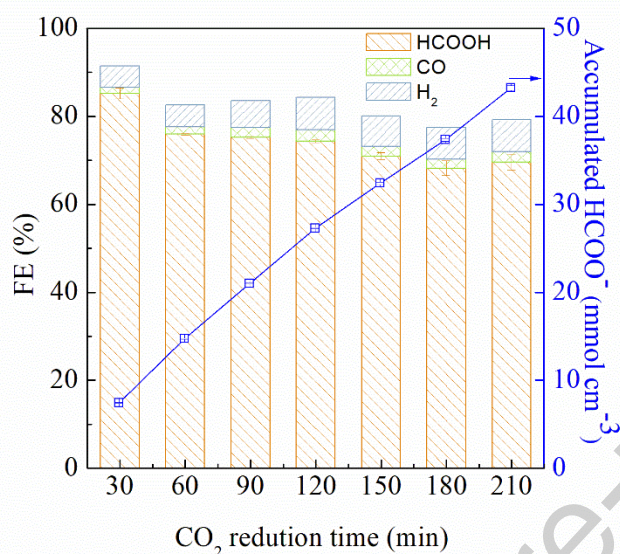


**Fig. 12.** Faradaic efficiencies and amount of accumulated  $\text{HCOO}^-$  during the electrolytic tests at  $-1.6 \text{ V}_{\text{SCE}}$  with Ag-Bi@GF in  $0.5 \text{ mol L}^{-1} \text{ KHCO}_3$  (pH 7.2) under  $\text{CO}_2$  saturation with one pass through the electrode. Flow rate:  $1 \text{ mL min}^{-1}$ . Error bars are based on two measurements.

SEM analysis was performed on the Ag-Bi@GF electrode after the 7<sup>th</sup> electrolysis (Fig. S6). The appearance of the Bi surface changed from a compact layer to thin nanosheets of Bi with different orientations. Moreover, EDS analysis showed the disappearance of Ag from the Bi surface, that could explain the decrease of the FE for formate from 85% to 70%, which is the mean value obtained with Bi@GF (Fig. 7). The removal of Ag particles from the Bi coated fibers can be attributed to gas ( $\text{H}_2$  and  $\text{CO}$ ) evolution during the electroreduction of  $\text{CO}_2$  and to the weak interactions between amorphous silver and bismuth. Indeed, the mechanical

stability of the electrode was ascertained by SEM/EDS analysis after flowing water through the porous electrode in the electrochemical cell for 24h at open circuit (Fig. S7). A better stability could be obtained if a lower potential was used. A good compromise has to be found between the stability and the FE of formate.

## Conclusions

A three-dimensional porous bismuth electrode with silver particles of 200-400 nm size was prepared from Bi-coated graphite felt by galvanic displacement reaction. The electrochemical reduction of CO<sub>2</sub> was investigated with Bi@GF and Ag-Bi@GF electrodes in a flow electrochemical cell with one pass of a 0.5 mol L<sup>-1</sup> KHCO<sub>3</sub> solution saturated with CO<sub>2</sub>. As it is usually obtained on bismuth electrode, the reduction occurred at -1.3 V<sub>SCE</sub> on Bi@GF. The reduction of CO<sub>2</sub> at Ag-Bi@GF electrode occurred at a 100 mV less negative potential. Although the reduction of CO<sub>2</sub> at Ag is known to give CO, the Ag-Bi@GF electrode was found to lead to a low amount of formed CO (1-2%) and to a higher FE for formate when compared with Bi@GF (88% against 70%). The complementary role of Ag and Bi in the catalytic mechanism could explain the higher FE for formate. At -1.6 V<sub>SCE</sub>, a surface current density of 76 mA cm<sup>-2</sup> and a production rate for formate of 62 mg cm<sup>-2</sup> were obtained. Such high values for a CO<sub>2</sub>-saturated solution are ascribed to the use of a porous electrode with high specific surface area. These preliminary results are very promising and could be improved by carrying out the reduction of CO<sub>2</sub> at Bi@GF and Ag-Bi@GF in a gas-diffusion cell to improve the concentration of CO<sub>2</sub> at the electrode surface.

### **CreditAuthorStatement**

**Yaoyin Lou:** Conceptualization; Data curation; Formal analysis; Investigation; Visualization; Writing - original draft; **Dong Fu:** Investigation **Bruno Fabre:** Resources; Supervision; Validation **Florence Fourcade:** Conceptualization; Funding acquisition; Resources; Supervision; Validation **Abdeltif Amrane:** Conceptualization; Funding acquisition; Project administration; Resources; Supervision; **Mathieu Pasturel:** Resources; Formal analysis; Investigation **Riadh Bourzami:** Formal analysis; Investigation **Odile Merdrignac-Conanec:** Resources; Formal analysis; Investigation **Thierry Labasque:** Resources; Formal analysis **Florence Geneste:** Conceptualization; Formal analysis; Funding acquisition; Project administration; Resources; Supervision; Validation; Visualization; Writing - review & editing.

### **Declaration of interests**

The authors declare that they have no known competing financial interests or personal relationships that could have appeared to influence the work reported in this paper.

### **Acknowledgements**

The Platforme “Condate Eau” (<https://condate-eau.univ-rennes1.fr>) is fully thanked for their help in the detection and quantification of CO and H<sub>2</sub> gases. Y. Y. Lou thanks the China Scholarship Council for a Ph. D. grant.

## References

- [1] A. Bard, *Standard potentials in aqueous solution.*, Routledge, 2017.
- [2] E.E. Barton, D.M. Rampulla, A.B. Bocarsly, Selective Solar-Driven Reduction of CO<sub>2</sub> to Methanol Using a Catalyzed p-GaP Based Photoelectrochemical Cell, *J. Am. Chem. Soc.*, 130 (2008) 6342-6344.
- [3] C.W. Li, J. Ciston, M.W. Kanan, Electroreduction of carbon monoxide to liquid fuel on oxide-derived nanocrystalline copper, *Nature*, 508 (2014) 504-507.
- [4] A.A. Peterson, F. Abild-Pedersen, F. Studt, J. Rossmeisl, J.K. Nørskov, How copper catalyzes the electroreduction of carbon dioxide into hydrocarbon fuels, *Energy Environ. Sci.*, 3 (2010) 1311-1315.
- [5] A.V. Rudnev, K. Kiran, A. Cedeno Lopez, A. Dutta, I. Gjurroski, J. Furrer, P. Broekmann, Enhanced electrocatalytic CO formation from CO<sub>2</sub> on nanostructured silver foam electrodes in ionic liquid/water mixtures, *Electrochim. Acta*, 306 (2019) 245-253.
- [6] C. Kim, H.S. Jeon, T. Eom, M.S. Jee, H. Kim, C.M. Friend, B.K. Min, Y.J. Hwang, Achieving Selective and Efficient Electrocatalytic Activity for CO<sub>2</sub> Reduction Using Immobilized Silver Nanoparticles, *J. Am. Chem. Soc.*, 137 (2015) 13844-13850.
- [7] M. Ma, B.J. Trzesniewski, J. Xie, W.A. Smith, Selective and Efficient Reduction of Carbon Dioxide to Carbon Monoxide on Oxide-Derived Nanostructured Silver Electrocatalysts, *Angew. Chem., Int. Ed.*, 55 (2016) 9748-9752.
- [8] Y.S. Ham, S. Choe, M.J. Kim, T. Lim, S.-K. Kim, J.J. Kim, Electrodeposited Ag catalysts for the electrochemical reduction of CO<sub>2</sub> to CO, *Appl. Catal., B*, 208 (2017) 35-43.
- [9] K.P. Kuhl, T. Hatsukade, E.R. Cave, D.N. Abram, J. Kibsgaard, T.F. Jaramillo, Electrocatalytic Conversion of Carbon Dioxide to Methane and Methanol on Transition Metal Surfaces, *J. Am. Chem. Soc.*, 136 (2014) 14107-14113.
- [10] A. Atifi, D.W. Boyce, J.L. Di Meglio, J. Rosenthal, Directing the Outcome of CO<sub>2</sub> Reduction at Bismuth Cathodes Using Varied Ionic Liquid Promoters, *ACS Catal.*, 8 (2018) 2857-2863.
- [11] J. Medina-Ramos, S.S. Lee, T.T. Fister, A.A. Hubaud, R.L. Sacci, D.R. Mullins, J.L. DiMeglio, R.C. Pupillo, S.M. Velardo, D.A. Lutterman, J. Rosenthal, P. Fenter, Structural Dynamics and Evolution of Bismuth Electrodes during Electrochemical Reduction of CO<sub>2</sub> in Imidazolium-Based Ionic Liquid Solutions, *ACS Catal.*, 7 (2017) 7285-7295.

- [12] M.C. Thompson, J. Ramsay, J.M. Weber, Solvent-Driven Reductive Activation of CO<sub>2</sub> by Bismuth: Switching From Metalloformate Complexes to Oxalate Products, *Angew. Chem., Int. Ed.*, 55 (2016) 14876.
- [13] P. Su, W. Xu, Y. Qiu, T. Zhang, X. Li, H. Zhang, Ultrathin Bismuth Nanosheets as a Highly Efficient CO<sub>2</sub> Reduction Electrocatalyst, *ChemSusChem*, 11 (2018) 848-853.
- [14] Z. Zhang, M. Chi, G.M. Veith, P. Zhang, D.A. Lutterman, J. Rosenthal, S.H. Overbury, S. Dai, H. Zhu, Rational Design of Bi Nanoparticles for Efficient Electrochemical CO<sub>2</sub> Reduction: The Elucidation of Size and Surface Condition Effects, *ACS Catal.*, 6 (2016) 6255-6264.
- [15] S. He, F. Ni, Y. Ji, L. Wang, Y. Wen, H. Bai, G. Liu, Y. Zhang, Y. Li, B. Zhang, H. Peng, The p-Orbital Delocalization of Main-Group Metals to Boost CO<sub>2</sub> Electroreduction, *Angew. Chem., Int. Ed.*, 57 (2018) 16114-16119.
- [16] H. He, C. Morrissey, L.A. Curtiss, P. Zapol, Graphene-Supported Monometallic and Bimetallic Dimers for Electrochemical CO<sub>2</sub> Reduction, *Journal of Physical Chemistry C*, 122 (2018) 28629-28636.
- [17] S. Zhao, R. Jin, R. Jin, Opportunities and Challenges in CO<sub>2</sub> Reduction by Gold- and Silver-Based Electrocatalysts: From Bulk Metals to Nanoparticles and Atomically Precise Nanoclusters, *ACS Energy Lett.*, 3 (2018) 452-462.
- [18] X. Zhang, F. Li, Y. Zhang, A.M. Bond, J. Zhang, Stannate derived bimetallic nanoparticles for electrocatalytic CO<sub>2</sub> reduction, *J. Mater. Chem. A*, 6 (2018) 7851-7858.
- [19] J. Huang, M. Mensi, E. Oveisi, V. Mantella, R. Buonsanti, Structural Sensitivities in Bimetallic Catalysts for Electrochemical CO<sub>2</sub> Reduction Revealed by Ag-Cu Nanodimers, *J. Am. Chem. Soc.*, 141 (2019) 2490-2499.
- [20] Z. Chang, S. Huo, W. Zhang, J. Fang, H. Wang, The Tunable and Highly Selective Reduction Products on Ag@Cu Bimetallic Catalysts Toward CO<sub>2</sub> Electrochemical Reduction Reaction, *Journal of Physical Chemistry C*, 121 (2017) 11368-11379.
- [21] M.Y. Zu, L. Zhang, C. Wang, L.R. Zheng, H.G. Yang, Copper-modulated bismuth nanocrystals alter the formate formation pathway to achieve highly selective CO<sub>2</sub> electroreduction, *J. Mater. Chem. A*, 6 (2018) 16804-16809.
- [22] W. Lv, J. Zhou, J. Bei, R. Zhang, L. Wang, Q. Xu, W. Wang, Electrodeposition of nano-sized bismuth on copper foil as electrocatalyst for reduction of CO<sub>2</sub> to formate, *Appl. Surf. Sci.*, 393 (2017) 191-196.

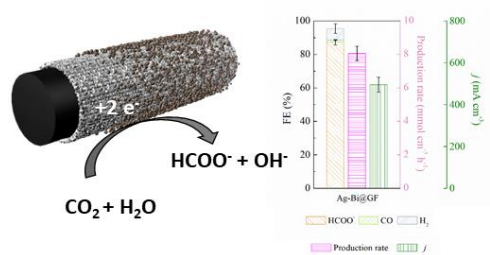
- [23] X. Sun, Q. Zhu, X. Kang, H. Liu, Q. Qian, Z. Zhang, B. Han, Molybdenum-Bismuth Bimetallic Chalcogenide Nanosheets for Highly Efficient Electrocatalytic Reduction of Carbon Dioxide to Methanol, *Angew. Chem., Int. Ed.*, 55 (2016) 6771-6775.
- [24] G. Wen, D.U. Lee, B. Ren, F.M. Hassan, G. Jiang, Z.P. Cano, J. Gostick, E. Croiset, Z. Bai, L. Yang, Z. Chen, Orbital Interactions in Bi-Sn Bimetallic Electrocatalysts for Highly Selective Electrochemical CO<sub>2</sub> Reduction toward Formate Production, *Adv. Energy Mater.*, 8 (2018) 1802427.
- [25] J.-H. Zhou, K. Yuan, L. Zhou, Y. Guo, M.-Y. Luo, X.-Y. Guo, Q.-Y. Meng, Y.-W. Zhang, Boosting Electrochemical Reduction of CO<sub>2</sub> at a Low Overpotential by Amorphous Ag-Bi-S-O Decorated BiO Nanocrystals, *Angew. Chem., Int. Ed.*, 58 (2019) 14197-14201.
- [26] M. Jouny, W. Luc, F. Jiao, General Techno-Economic Analysis of CO<sub>2</sub> Electrolysis Systems, *Ind. Eng. Chem. Res.*, 57 (2018) 2165-2177.
- [27] S. Verma, Y. Hamasaki, C. Kim, W. Huang, S. Lu, H.-R.M. Jhong, A.A. Gewirth, T. Fujigaya, N. Nakashima, P.J.A. Kenis, Insights into the Low Overpotential Electroreduction of CO<sub>2</sub> to CO on a Supported Gold Catalyst in an Alkaline Flow Electrolyzer, *ACS Energy Lett.*, 3 (2018) 193-198.
- [28] J.-J. Lv, M. Jouny, W. Luc, W. Zhu, J.-J. Zhu, F. Jiao, A Highly Porous Copper Electrocatalyst for Carbon Dioxide Reduction, *Adv. Mater.*, 30 (2018) 1803111.
- [29] F. Geneste, Catalytic electrochemical pre-treatment for the degradation of persistent organic pollutants, *Curr. Opin. Electrochem.*, 11 (2018) 19-24.
- [30] R. Abdallah, F. Geneste, T. Labasque, H. Djelal, F. Fourcade, A. Amrane, S. Taha, D. Floner, Selective and quantitative nitrate electroreduction to ammonium using a porous copper electrode in an electrochemical flow cell, *J. Electroanal. Chem.*, 727 (2014) 148-153.
- [31] Y.-Y. Lou, W. He, E. Verlato, M. Musiani, D. Floner, F. Fourcade, A. Amrane, C. Li, Z.-Q. Tian, O. Merdrignac-Conanec, N. Coulon, F. Geneste, Ni-coated graphite felt modified with Ag nanoparticles: a new electrode material for electro-reductive dechlorination, *J. Electroanal. Chem.*, 849 (2019) 113357.
- [32] R. Abdallah, A. Derghane, Y.-Y. Lou, O. Merdrignac-Conanec, D. Floner, F. Geneste, New porous bismuth electrode material with high surface area, *J. Electroanal. Chem.*, 839 (2019) 32-38.
- [33] Y.-Y. Lou, P. Hapiot, D. Floner, F. Fourcade, A. Amrane, F. Geneste, Efficient dechlorination of  $\alpha$ -halocarbonyl and  $\alpha$ -haloallyl pollutants by electroreduction on bismuth, *Environ. Sci. Technol.*, 54 (2020) 559-567.

- [34] E. Verlato, W. He, A. Amrane, S. Barison, D. Floner, F. Fourcade, F. Geneste, M. Musiani, R. Seraglia, Preparation of Silver-Modified Nickel Foams by Galvanic Displacement and Their Use as Cathodes for the Reductive Dechlorination of Herbicides, *ChemElectroChem*, 3 (2016) 2084-2092.
- [35] J.M. Fontmorin, W.Y. He, D. Floner, F. Fourcade, A. Amrane, F. Geneste, Reductive dehalogenation of 1,3-dichloropropane by a [Ni(tetramethylcyclam)]Br<sub>2</sub>-Nafion modified electrode, *Electrochim. Acta*, 137 (2014) 511-517.
- [36] W. He, Y. Lou, E. Verlato, I. Soutrel, D. Floner, F. Fourcade, A. Amrane, M. Musiani, F. Geneste, Reductive dehalogenation of a chloroacetanilide herbicide in a flow electrochemical cell fitted with Ag-modified Ni foams, *J. Chem. Technol. Biotechnol.*, 93 (2018) 1572-1578.
- [37] B. Liu, C. Ding, B. Xiao, L. Cui, M. Wang, Electrocatalytic dechlorination of chloroacetic acids on silver nanodendrites electrode, *Mater. Sci. Eng., C*, 37 (2014) 108-112.
- [38] X. Xia, J. Zeng, L.K. Oetjen, Q. Li, Y. Xia, Quantitative Analysis of the Role Played by Poly(vinylpyrrolidone) in Seed-Mediated Growth of Ag Nanocrystals, *J. Am. Chem. Soc.*, 134 (2012) 1793-1801.
- [39] H. Zhang, Y. Ma, F. Quan, J. Huang, F. Jia, L. Zhang, Selective electro-reduction of CO<sub>2</sub> to formate on nanostructured Bi from reduction of BiOCl nanosheets, *Electrochem. Commun.*, 46 (2014) 63-66.
- [40] M. Dunwell, Q. Lu, J.M. Heyes, J. Rosen, J.G. Chen, Y. Yan, F. Jiao, B. Xu, The Central Role of Bicarbonate in the Electrochemical Reduction of Carbon Dioxide on Gold, *J. Am. Chem. Soc.*, 139 (2017) 3774-3783.
- [41] N.S. Lewis, G.A. Shreve, Photochemical and Photoelectrochemical Reduction of Carbon Dioxide in: B.R. Sullivan, K. Krist, H.E. Guard (Eds.) *Electrochemical and Electrocatalytic Reactions of Carbon Dioxide*, Elsevier science publishers B.V. , 1993, pp. 263-289.
- [42] N. Han, Y. Wang, H. Yang, J. Deng, J. Wu, Y. Li, Y. Li, Ultrathin bismuth nanosheets from in situ topotactic transformation for selective electrocatalytic CO<sub>2</sub> reduction to formate, *Nat. Commun.*, 9 (2018) 1-8.
- [43] D. Higgins, C. Hahn, C. Xiang, T.F. Jaramillo, A.Z. Weber, Gas-Diffusion Electrodes for Carbon Dioxide Reduction: A New Paradigm, *ACS Energy Lett.*, 4 (2019) 317-324.
- [44] N. Yang, S.R. Waldvogel, X. Jiang, Electrochemistry of Carbon Dioxide on Carbon Electrodes, *ACS Appl. Mater. Interfaces*, 8 (2016) 28357-28371.

[45] W. Oh, C.K. Rhee, J.W. Han, B. Shong, Atomic and Molecular Adsorption on the Bi(111) Surface: Insights into Catalytic CO<sub>2</sub> Reduction, *Journal of Physical Chemistry C*, 122 (2018) 23084-23090.

Journal Pre-proof

## Graphical abstract



Journal Pre-proof